PHYSICAL REVIEW B **79**, 165309 (2009)

Nonlinear dynamics and chaos in two coupled nanomechanical resonators

R. B. Karabalin, M. C. Cross, and M. L. Roukes
Department of Physics and Kavli Nanoscience Institute, California Institute of Technology, Pasadena, California 91125, USA
(Received 10 February 2009; published 13 April 2009)

Two elastically coupled nanomechanical resonators driven independently near their resonance frequencies show intricate nonlinear dynamics. The dynamics provide a scheme for realizing a nanomechanical system with tunable frequency and nonlinear properties. For large vibration amplitudes, the system develops spontaneous oscillations of amplitude modulation that also show period-doubling transitions and chaos. The complex nonlinear dynamics are quantitatively predicted by a simple theoretical model.

DOI: 10.1103/PhysRevB.79.165309 PACS number(s): 85.85.+j, 05.45.−a, 62.25.−g

I. INTRODUCTION

Resonant nanoelectromechanical systems (NEMS)[1] are attracting interest in a broad variety of research areas and for many possible applications due to their remarkable combination of properties: small mass, high operating frequency, large quality factor, and easily accessible nonlinearity.[2] Further development of NEMS applications, such as superior mass,[3] force,[4] and charge[5] sensors, or reaching the quantum limit of detection in mechanical systems,[6] requires addressing several important challenges. For example, the nonlinearity of the devices has to be either minimized or utilized for improving performance.[7] In addition, the large-scale integration of nanodevices demands a detailed understanding of the behavior of coupled devices in NEMS arrays.[8–11]

In this paper we demonstrate the complex nonlinear behavior of a pair of coupled nanomechanical devices that can be quantitatively understood from the basic physics of the devices. We show that the linear and weakly nonlinear response of one oscillation can be modified by driving the second oscillation and that the linear-response range of the first oscillation can be significantly extended. When both oscillations are driven into their strongly nonlinear range, more complicated frequency-sweep response curves are found, corresponding to the well-known bistability of driven anharmonic "Duffing" resonators, but now with switching between a variety of different stable states of the coupled pair not seen previously. Spontaneous amplitude modulation oscillations may develop, with frequencies characteristic of the dissipation rates rather than of the intrinsic frequencies or their sums and differences. These amplitude modulations show period-doubling bifurcations and chaos, giving a clear demonstration of these complex dynamics in the context of nanomechanical systems.[12] The complex dynamics are reproduced quantitatively by a simple theoretical model.

II. EXPERIMENTAL SETUP

We study a system of two strongly coupled nonlinear nanoelectromechanical resonators using a structure of doubly clamped beams with a shared mechanical ledge shown in Fig. 1(a). The devices consist of a stack of three layers of gallium arsenide (GaAs): a 100 nm highly *n*-doped layer, a 50 nm insulating layer, and another 50 nm layer that is highly *p* doped. The piezoelectric property of GaAs results in a highly efficient integrated actuation mechanism described in Ref. 13. A preliminary 120-nm-deep etch step is done to isolate the actuation electrodes of the two beams, so that the two beams can be addressed separately while retaining strong elastic coupling.

Optical interferometry is used for the motion transduction.[14] The GaAs heterostructures are epitaxially grown on a nearly perfectly lattice-matched sacrificial layer of $Al_{0.8}Ga_{0.2}As$, which can be removed with a high degree of selectivity to reveal a smooth substrate that forms a mirror. The top surface of the NEMS device forms a second mirror. Coupled together, the mirrors produce a primitive Fabry-Pérot interference cavity. The reflection coefficient for light that is normally incident on a vacuum-GaAs interface is about 33% and because of the relatively low light intensity, it is sufficient to consider a single reflection from each surface. An infrared laser diode (904 nm) followed by an attenuator is used as the light source. Its frequency is below the band gap of GaAs (830 nm), in order to minimize heating and photocurrent generation. The beam is focused onto the nano-

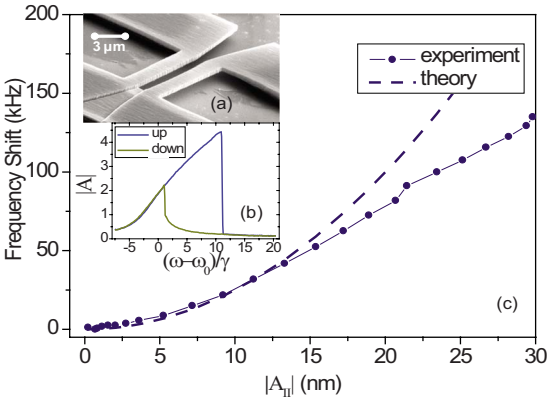

FIG. 1. (Color online) (a) SEM image of the system (beam dimensions: 6 μm × 500 nm × 200 nm). (b) Up (dark, blue) and down (light, yellow) frequency sweeps of the amplitude $|A|$ of the response for a single drive of strength 4.3 times critical as a function of the frequency relative to the linear resonance frequency ω_0 and scaled by the width γ. The amplitude is plotted in units of the maximum amplitude at the critical drive strength. (c) Frequency shift of the weakly driven first mode as a function of the displacement amplitude $|A_{II}|$ of the strongly driven second mode: points and solid line—experiment; dashed line—small amplitude theory.

mechanical device with a lens of numerical aperture 0.15, giving a spot size of approximately 10 μm. The laser beam is adjusted so that both beams are in the illuminated spot. After reflection from the top surface of the mechanical resonator and the bottom mirror, the beam intensity is modulated proportional to the mechanical displacement. A high-bandwidth low-noise photodetector is used to measure the intensity of the light and thus the mechanical displacement of the resonators.

III. THEORETICAL MODEL

We model the behavior of the two strongly interacting nonlinear resonators by a system of coupled equations of motion for the beam displacements x_1, x_2 in their fundamental modes

$$\ddot{x}_1 + \gamma_1 \dot{x}_1 + \omega_1^2 x_1 + \alpha_1 x_1^3 + D(x_1 - x_2) = g_{D1}(t), \quad (1)$$

$$\ddot{x}_2 + \gamma_2 \dot{x}_2 + \omega_2^2 x_2 + \alpha_2 x_2^3 + D(x_2 - x_1) = g_{D2}(t). \quad (2)$$

As well as the usual terms describing the resonant frequencies, damping, and Duffing nonlinearity, we include a linear coupling term in the displacements of strength D. The terms on the right-hand side are the external drives applied to the two beams, which are controlled independently. The linear terms in the equations, ignoring for now the drive and dissipation, give two modes with frequencies ω_{I} and ω_{II} and corresponding eigenvectors $\mathbf{e}_{\mathrm{I}}, \mathbf{e}_{\mathrm{II}}$.[15] The frequency difference of the modes results from both the intrinsic frequency difference ω_1-ω_2 and the coupling D.

To investigate the behavior of the system, the two beams are connected to two different sources with independent frequencies and amplitudes. The monitored output variables are the amplitudes and phases of a linear combination of the mechanical displacements of the two beams at or near the two drive frequencies.[16] By applying various combinations of small amplitude signals to the two beams at frequencies near the mode resonances, the linear coupling parameters can be determined. For the particular device shown in Fig. 1(a), the mode frequencies are determined to be $\omega_{\mathrm{I}}/2\pi = 16.79$ MHz and $\omega_{\mathrm{I}}/2\pi = 17.25$ MHz and the eigenvectors $\mathbf{e}_{\mathrm{I}} = (0.854, 0.521)$ and $\mathbf{e}_{\mathrm{II}} = (-0.521, 0.854)$. The frequencies of the individual resonators determined from inverting the mode equations are $\omega_1/2\pi = 16.71$ MHz and $\omega_2/2\pi = 16.92$ MHz. The frequency separation of 200 kHz is consistent with the fabrication tolerance. The coupling strength $\sqrt{D}/2\pi = 2.63$ MHz is consistent with the strength of the elastic coupling found by finite element simulations of similar devices.[17] Transforming the measured width of the modes back to the original equations determines the values of γ_1, γ_2. The nonlinear parameters α_1, α_2 are deduced from the expression for the geometric nonlinearity[7] using the beam thickness known from the fabrication and lengths calculated from the beam frequencies ω_1, ω_2 and the material constants.[18]

The response of the system driven near resonance and for small dissipation and driving can be calculated from Eqs. (1) and (2) using the standard methods of secular perturbation theory.[2] This approach has previously used for the case of parametrically driven nanomechanical devices,[9–11] where hysteretic switches between different stable states in frequency sweeps were also predicted. Briefly, we introduce the slowly varying complex mode amplitudes $A_{\mathrm{I}}, A_{\mathrm{II}}$ and forces $F_{\mathrm{I}}, F_{\mathrm{II}}$ using $x_{[\mathrm{I}]} = \mathrm{Re}(A_{[\mathrm{I}]} e^{i\omega_{[\mathrm{I}]} t})$ and $g_{D[\mathrm{I}]} = \mathrm{Re}[F_{[\mathrm{I}]}(t) e^{i\omega_{[\mathrm{I}]} t}]$ (where [I] stands for either I or II), substitute into the equations of motion, and retain only the near resonant terms. This reduces the equations of motion to

$$2i\omega_{\mathrm{I}} \dot{A}_{\mathrm{I}} + i\omega_{\mathrm{I}} \gamma_{\mathrm{I}} A_{\mathrm{I}} + \alpha_{\mathrm{I}} |A_{\mathrm{I}}|^2 A_{\mathrm{I}} + \beta_{\mathrm{I}} |A_{\mathrm{II}}|^2 A_{\mathrm{I}} = F_{\mathrm{I}}(t), \quad (3)$$

and a corresponding equation for A_{II}. The mode nonlinearity parameters $\alpha_{[\mathrm{I}]}$ and $\beta_{[\mathrm{I}]}$ are calculated from α_1, α_2 and the eigenvectors $\mathbf{e}_{\mathrm{I}}, \mathbf{e}_{\mathrm{II}}$ so that all the parameters in Eq. (3) are known from linear measurements and the beam geometry and material constants.

IV. RESULTS

We first look at the case where each mode responds at the drive frequency $\omega_{D[\mathrm{I}]}$ which is set near the resonant frequency $\omega_{[\mathrm{I}]}$ so that $A_{[\mathrm{I}]} \propto e^{i(\omega_{D[\mathrm{I}]} - \omega_{[\mathrm{I}]})t}$, with

$$|A_{\mathrm{I}}|^2 = \frac{|F_{\mathrm{I}}|^2}{[2\omega_{\mathrm{I}}(\omega_{D\mathrm{I}} - \omega_{\mathrm{I}}) - \alpha_{\mathrm{I}}|A_{\mathrm{I}}|^2 - \beta_{\mathrm{I}}|A_{\mathrm{II}}|^2]^2 + \omega_{\mathrm{I}}^2 \gamma_{\mathrm{I}}^2}, \quad (4)$$

etc. For a single drive (e.g., $A_{\mathrm{II}} = F_{\mathrm{II}} = 0$), so that the cross-mode nonlinear coupling proportional to $\beta_{[\mathrm{I}]}$ is not involved, this expression reproduces the regular Duffing response curve.[19] Prominent features are the shift of the frequency of the maximum response to larger values for positive α (nonlinear spring stiffening) and bistability and hysteresis that develop above a critical drive strength. An experimental example of upward and downward frequency sweeps for a drive strength 4.3 times critical is shown in Fig. 1(b).

We first look at the linear and weakly nonlinear responses of the first mode when the second mode is driven into its strongly nonlinear regime. Retaining the leading-order effect of the first mode on the intensity of the second mode, we can write the numerator in Eq. (4) as

$$[2\omega_{\mathrm{I}}(\omega_{D\mathrm{I}} - \omega_{\mathrm{I}}) - \beta_{\mathrm{I}}|A_{\mathrm{II}}^{(0)}|^2 - \bar{\alpha}_I |A_{\mathrm{I}}|^2]^2 + \omega_{\mathrm{I}}^2 \gamma_{\mathrm{I}}^2, \quad (5)$$

where $A_{\mathrm{II}}^{(0)}$ is the solution for the second mode in the absence of mode I given by the equation for A_{II} corresponding to Eq. (4) assuming zero A_{I}. The parameter $\bar{\alpha}_{\mathrm{I}}$ is an effective Duffing nonlinearity coefficient and is given by

$$\bar{\alpha}_{\mathrm{I}} = \alpha_{\mathrm{I}} - 2\beta_{\mathrm{I}}\beta_{\mathrm{II}}\omega_{\mathrm{II}}\, \partial |A_{\mathrm{II}}^{(0)}|^2 / \partial \omega_{D\mathrm{II}}. \quad (6)$$

The expression (5) predicts two important effects: the frequency tuning of the first mode proportional to the square of the amplitude of the second mode (upwards for positive β_{I}) and the change in the effective nonlinear coefficient for the motion of the first mode depending on the excitation strength of the second mode through the last term in $\bar{\alpha}_{\mathrm{I}}$ Eq. (6).

To test the frequency tuning, we excite the second mode at a drive level approximately 4.3 times the critical value so that the spectral response is the strongly nonlinear Duffing curve [see Fig. 1(b)]. As the actuation frequency of the sec-

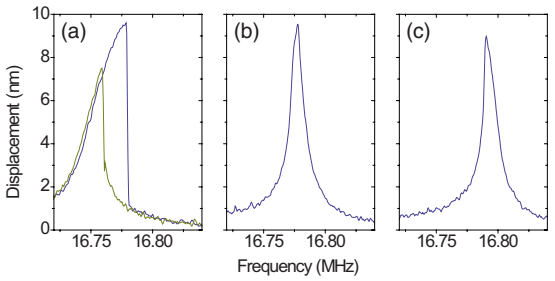

FIG. 2. (Color online) Frequency sweeps of the first mode response for increasing amplitudes of the second mode: the dark (blue) lines are for upward sweeps; the light (yellow) line in (a) is a downward sweep, showing the hysteresis and amplitude jumps in this case. There are no hysteretic jumps for (b) and (c), and so the downward sweeps are not shown.

ond mode is steadily increased in small steps, its vibration amplitude rises over a wide frequency range until it drops to the lower amplitude state beyond the maximum. The evolution of the spectral response of the first mode is monitored at a driving level approximately four times lower than the critical value for this mode using a network analyzer. The dependence of the first mode frequency shift on the vibration amplitude of the second mode is shown in Fig. 1(c). The experimental results for frequency tuning closely follow the predicted parabolic dependence $\beta_{\mathrm{I}}|A_{\mathrm{II}}|^2$ for amplitudes up to about 20 nm.

If the actuation level of the first mode is increased above the onset of nonlinearity, while the second mode drive is kept at a much higher level then the effective nonlinear coefficient $\bar{\alpha}_{\mathrm{I}}$ is decreased. The decrease is largest when the second mode is driven on the portion of the Duffing response curve where the intensity is increasing linearly with the drive frequency $|A_{\mathrm{II}}|^2 \simeq 2\omega_{\mathrm{II}}(\omega_{D\mathrm{II}}-\omega_{\mathrm{II}})/\alpha_{\mathrm{II}}$. This gives the minimum effective nonlinear coefficient

$$\bar{\alpha}_{\mathrm{I,min}} = \alpha_{\mathrm{I}}\left(1 - \frac{\beta_{\mathrm{I}}\beta_{\mathrm{II}}}{\alpha_{\mathrm{I}}\alpha_{\mathrm{II}}}\right). \tag{7}$$

This result indicates that if the coupling is strong enough, so that $\beta_{\mathrm{I}}\beta_{\mathrm{II}} > \alpha_{\mathrm{I}}\alpha_{\mathrm{II}}$, the minimum value of the effective nonlinear coefficient is negative. In this case the resonance curve tilts to the left, as opposed to the usual case for a doubly clamped beam where the peak leans to the right. It also means that the nonlinear coefficient vanishes for some drive strength and frequency of the second mode.

Some experimental results for the first mode driven at twice the critical strength illustrating this effect are shown in Fig. 2. The plots show the shape of the resonance peak for three values of the drive frequency of the second mode. In panel (a), the amplitude A_{II} of the second mode is low and the first mode spectral response has the regular nonlinear Duffing shape leaning to the right. For larger A_{II} as in (b), the first mode resonance peak shape assumes a form close to a Lorentzian with little nonlinearity apparent. For even larger A_{II} as in (c), the sign of the effective Duffing coefficient becomes slightly negative, causing the spectral response peak to lean to the left. The quenching of the nonlinearity in

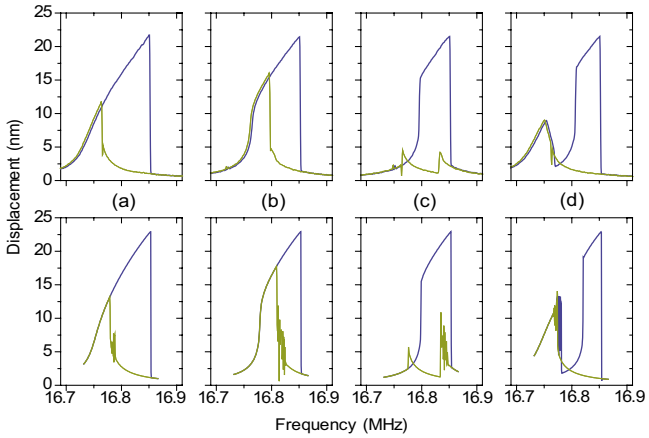

FIG. 3. (Color online) First mode frequency response as in Fig. 2 for increasing values of the second mode drive frequency but for stronger driving of the first mode (both modes are driven at about four times the critical strength). The top plots are experimental measurements while the bottom ones are theoretical simulations. The second mode response was monitored but is not shown.

(b) could be used to enhance the limited dynamic range[7] of nanomechanical devices.

If the drive level of the first mode is increased further, a variety of new effects can be observed. Under these conditions the dynamics of the system is not fully explained by the steady-state solutions as in Eq. (4), and so we solve for the expected behavior by numerically integrating the time-dependent coupled Eq. (3) and the corresponding equation for A_{II}. Now the behavior is more complex, as the response of the first mode becomes large enough to cause transitions in the second mode response through the nonlinear coupling. As a result, the spectral response curves acquire peculiar nontrivial shapes, as shown in Fig. 3. Numerical simulations of the equations give good predictions for the complex phenomena.

Figure 3 shows frequency sweeps of the first mode resonance for four increasing drive frequencies of the second mode. (The second mode response was monitored, but is not shown in the figure.) The top four plots are the experimental measurements and the bottom four are the numerical simulations. In panel (a) for experiment and theory, the second mode response is small, and the sweep of the first mode shows approximately the hysteretic response of a single Duffing oscillator. The interaction with the second mode is more important in the succeeding panels. For panels (b) and (c), on the upward sweep the amplitude of the second mode is initially large, which shifts the first mode response to larger frequencies, and gives a negative effective nonlinearity leading to a jump of the first mode to a larger amplitude as the frequency is swept up. This large amplitude is then sufficient to cause the second mode to transition to a lower amplitude, so that the remainder of the first mode sweep is close to the single mode Duffing curve. The downward sweeps in panels (b) and (c) are different depending on whether the second mode transitions between small and large amplitude states. In panel (d), the second mode amplitude is initially small on the upward sweep, and the first mode follows the single oscillator Duffing curve. This continues until the second mode

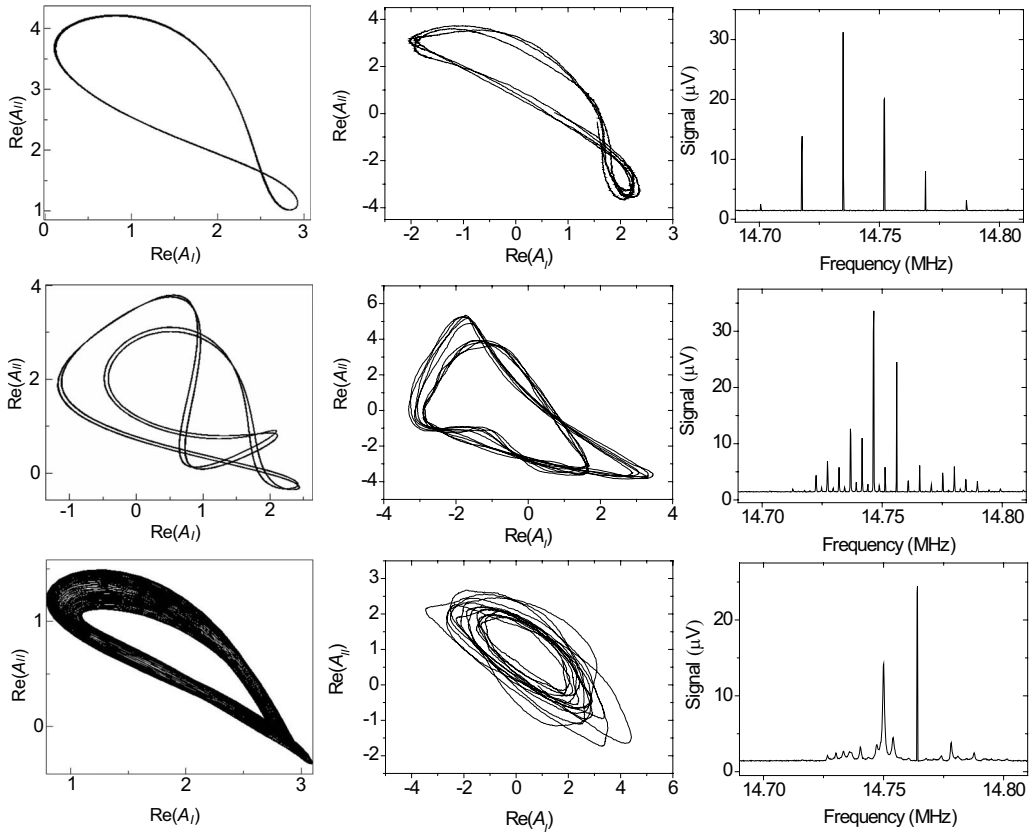

FIG. 4. Complex dynamics of two strongly coupled nanomechanical resonators. The three rows correspond to different input parameters (drive frequencies and amplitudes). The first column shows the theoretical calculation of the phase portrait, the second shows its experimental measurement, and the third column shows the corresponding experimental power spectrum of the optical measurement near one of the drive frequencies.

transitions to a large amplitude so that the first mode response jumps down and follows a curve close to the one in panel (c). The simple nonlinear model explains the complex behavior of the coupled system both qualitatively and quantitatively with a precision of better than 5%.

An obvious difference between the experimental and theoretical plots in Fig. 3 is the noisy regions on the theoretical curves near the up and down transitions. This difference actually results from the different ways the plots are generated in theory and experiment, and a more careful investigation shows consistent and interesting dynamics in both experiment and theory. It turns out that for the drive frequencies near the transition points, the fast (about 17 MHz) oscillating response becomes amplitude modulated with a frequency of about 10–20 kHz.[20] The theoretical simulations show that the frequency for the amplitude modulation is determined by the line width, which in our experimental setup is about 8 kHz, and is not related to sum and difference frequencies of the two modes. Examples of simulated and measured amplitude modulation dynamics for three different sets of drive parameters are shown in Fig. 4 for a second device with different parameters to the one used for Figs. 1–3. The first column shows examples of numerically calculated phase portraits of Re A_{II} versus Re A_{I} obtained by solving the time-dependent Eq. (3). Phase portraits measured experimentally are shown in the second column. These are obtained using homodyne down conversion of the transduced mechanical signals from both modes, which are then read by independent oscilloscope channels. We also perform wider frequency band spectrum analyzer measurements shown in the third column. Since the nature of the dynamics is sensitive to the precise values of the system parameters, the drive strength and frequencies in the experiment are slightly adjusted from the values corresponding to the theoretical plots to produce comparable phase portraits.

The top row of Fig. 4 shows a relatively simple example where the motion is periodic but the A_{I}-A_{II} trajectory forms a small figure-of-eight loop. The dynamics can be roughly understood in terms of transitions between states with the first mode at large amplitude and the second mode at small amplitude and vice versa. The spectrum of the measured mechanical signal shows satellite peaks corresponding to the anharmonic amplitude modulation.

As the parameters of the system are changed, we have observed period doubling or quadrupling in the amplitude modulation, where the phase trajectory takes two or four revolutions in order to complete the cycle.[21] An example of period quadrupling is shown in the middle row of Fig. 4. The complicated loop structures are visible in both theoretical and experimental trajectories, and the spectrum reveals amplitude modulation peaks at frequencies that correspond to double and quadruple periods. Period-doubling transitions are often associated with chaotic dynamics,[21] and indeed for other parameter values we observe chaos in our coupled na-

noelectromechanical system and in the theoretical model, as shown in the bottom row of Fig. 4. The evidence for the chaotic dynamics in the experiment is the broad band component to the spectrum (evident in the shoulders to the amplitude modulation peaks) and a phase portrait trajectory that does not form a closed loop. The theoretical model shows a similar phase portrait.

V. CONCLUSIONS

The complex dynamics we observe in coupled nanomechanical beam resonators have a number of potential applications. For example, driving one of the modes can be used to tune the effective nonlinearity of the other mode. This can be used to significantly increase the dynamic range of the resonator by quenching the effective nonlinearity. In a first approximation, the motion of one mode couples quadratically to the resonance frequency of the other mode: a phenomenon that has been proposed for quantum nondemolition measurements in nanomechanical systems.[22,23] The full range of complex dynamics investigated is quantitatively reproduced by theory, giving us confidence that the nonlinear behavior of coupled nanomechanical devices can be understood, controlled, and exploited. Applying these methods to large arrays of nanomechanical resonators that can be fabricated in the near future will enable the quantitative investigation of fundamental issues in the nonlinear dynamics of large numbers of coupled devices.

ACKNOWLEDGMENTS

Many of the ideas leading to this work were developed in collaboration with Ron Lifshitz supported by the U.S.-Israel Binational Science Foundation (BSF) through Grant No. 2004339. We would like to thank Iwijn De Vlaminck and Gustaaf Borghs from IMEC (Leuven, Belgium) for providing us with the GaAs material. We thank Matt Matheny for many useful discussions.

[1] M. L. Roukes, Phys. World **14**, 25 (2001).
[2] For a review, see R. Lifshitz and M. C. Cross, *Reviews of Nonlinear Dynamics and Complexity*, edited by H. G. Shuster (Wiley, Weinheim, 2008), Chap. 1, p. 52.
[3] Y. T. Yang, C. Calegari, X. L. Feng, K. L. Ekinci, and M. L. Roukes, Nano Lett. **6**, 583 (2006).
[4] D. Rugar, R. Budakian, H. J. Mamin, and B. W. Chui, Nature (London) **430**, 329 (2004).
[5] A. N. Cleland and M. L. Roukes, Nature (London) **392**, 160 (1998).
[6] M. D. Lahaye, O. Buu, B. Camarota, and K. C. Schwab, Science **304**, 74 (2004).
[7] H. W. C. Postma, I. Kozinsky, A. Husain, and M. L. Roukes, Appl. Phys. Lett. **86**, 223105 (2005).
[8] E. Buks and M. L. Roukes, Europhys. Lett. **54**, 220 (2001).
[9] R. Lifshitz and M. C. Cross, Phys. Rev. B **67**, 134302 (2003).
[10] Y. Bromberg, M. C. Cross, and R. Lifshitz, Phys. Rev. E **73**, 016214 (2006).
[11] E. Kenig, R. Lifshitz, and M. C. Cross, arXiv:0808.3589 (unpublished).
[12] Previous experiments by Scheible *et al.* [D. V. Scheible, A. Erbe, R. H. Blick, and G. Corso, Appl. Phys. Lett. **81**, 1884 (2002)], that suggested chaos in a nanomechanical system demonstrated a complex behavior of the response at one of the drive frequencies as that parameter was swept, rather than complex dynamics for fixed system parameters as shown in our work.
[13] S. C. Masmanidis, R. B. Karabalin, I. Vlaminck, G. Borghs, M. R. Freeman, and M. L. Roukes, Science **317**, 780 (2007).
[14] D. W. Carr and H. G. Craighead, J. Vac. Sci. Technol. B **15**, 2760 (1997).
[15] H. Goldstein, C. Poole, and J. Safko, *Classical Mechanics*, 3rd ed. (Addison-Wesley, New York, 2001).
[16] The combination measured depends on the geometry of the optical spot relative to the beams, which we determine from the linear experiments using a variety of drive combinations.
[17] R. B. Karabalin, Ph.D. dissertation, Caltech, 2008.
[18] The structure of the dynamical system depends on the ratio $\alpha_{\mathrm{I}}/\alpha_{\mathrm{II}}$ which is close to unity for our nearly identical beams. The absolute magnitude of α [approximately $0.007\ 2(\mathrm{MHz/nm})^2$] determines an overall proportionality constant in the driving strengths and calibrates the amplitude of the response in nanometer.
[19] A. H. Nayfeh and D. T. Mook, *Nonlinear Oscillations* (Wiley, New York, 1979).
[20] The theoretical points, which are the end values of a long numerical simulation, depend on the phase of the amplitude modulation at the end of each run, whereas this modulation simply leads to a drop in the experimentally measured amplitude since RF power is transferred outside the measurement bandwidth of the network analyzer.
[21] S. H. Strogatz, *Nonlinear Dynamics and Chaos* (Addison-Wesley, New York, 1994).
[22] K. C. Schwab and M. L. Roukes, Phys. Today **58**(7), 36 (2005).
[23] V. B. Braginsky and F. Y. Khalili, *Quantum Measurement* (Cambridge University Press, Cambridge, 1995).